Transient transport experiments in the current-drive experiment upgrade spherical torus

T. Munsat,[a] P. C. Efthimion, B. Jones, R. Kaita, R. Majeski, D. Stutman, and G. Taylor
Plasma Physics Laboratory, Princeton University, Princeton, New Jersey 08543

(Received 5 June 2001; accepted 24 October 2001)

Electron transport has been measured in the Current-Drive Experiment Upgrade (CDX-U) (T. Jones, Ph.D. thesis, Princeton University, 1995) using two separate perturbative techniques. Sawteeth at the $q=1$ radius ($r/a\sim0.15$) induced outward-propagating heat pulses, providing time-of-flight information leading to a determination of χ_e as a function of radius. Gas modulation at the plasma edge introduced inward-propagating cold pulses, providing a complementary time-of-flight based χ_e profile measurement. This work represents the first localized measurement of χ_e in a spherical torus. Core ($r/a<1/3$) χ_e values from the sawtooth study are $1-2$ m^2/s, and from the gas modulation study are $1-6$ m^2/s, increasing by an order of magnitude or more outside of the core region. Furthermore, the χ_e profile exhibits a sharp transition near $r/a=1/3$. Spectral and profile analyses of the soft x-rays, scanning interferometer, and edge probe data show no evidence of a significant magnetic island causing the high χ_e region. Comparisons are performed to several theoretical models, with measured $\chi_e\approx5-10\times$ neoclassical estimates in the core. © *2002 American Institute of Physics*. [DOI: 10.1063/1.1428557]

I. INTRODUCTION

In recent years there has been increased interest in the spherical torus (ST) geometry as a means of obtaining high fusion power density at relatively modest magnetic field.[1,2] Ideal magnetohydrodynamic (MHD) studies have found stable equilibria in this configuration featuring $\beta\sim50\%$ and pressure-driven bootstrap current fractions of $f_{BS}\sim100\%$,[3–5] and the Small Tight Aspect Ratio Tokamak (START) ST has achieved $\beta\sim30\%$ in the laboratory.[6,7] Additionally, certain MHD instabilities have been predicted to stablize as the aspect ratio (R/a) falls below 1.5.[2,8]

Confinement predictions for the ST geometry have been more sparse, though, with most studies limited to the application of global confinement scalings originally developed for conventional tokamaks.[9,10] This will change in the coming years, with the introduction of the large ST experiments National Spherical Torus Experiment (NSTX)[11] at Princeton Plasma Physics Laboratory (PPPL) and Mega Amp Spherical Tokamak (MAST)[12] at Culham. Transport studies are of utmost importance to the development of the ST as a candidate fusion reactor, since many of the most promising MHD phenomena depend on highly tailored pressure and current profiles.

The entire collection of thermal transport data in ST's up to now can be covered by summarizing the results from the START device ($I_P\sim200$ kA, $B_T\sim4-6$ kG, $T_e\sim300-500$ eV, $R/a=1.3-1.5$),[13] including both ohmic and neutral beam injection (NBI) heated plasmas. Global confinement studies of ohmic START plasmas have shown $\tau_E\sim0.5-1.2$ ms,[14] with reasonable agreement found with the semiempirical modified Lackner–Gottardi model.[15,16] Calculation of χ_e profiles based on power-balance considerations were performed for high-performance neutral-beam-injected (NBI) heated START discharges, resulting in estimates of $\chi_e\sim20$ m^2/s and $\chi_i\sim5-10$ m^2/s.[7] Again a reasonable agreement was found between the magnitude of χ_e and Lackner–Gottardi estimates, though the profile shape showed a poor match to the model. χ_i was found to be in reasonable agreement with Chang–Hinton neoclassical estimates. Neoclassical χ_e estimates were not performed.

In the present experiment, perturbative techniques are used in the Current-Drive Experiment Upgrade (CDX-U) ST[17] ($I_P\sim70$ kA, $B_T\sim2.3$ kG, $T_e\sim100$ eV, $R_0=34$ cm, $a=22$ cm, $A=R_0/a=1.5$) to derive localized measurements of the χ_e profile.

Perturbative transport experiments have been performed on nearly all major fusion devices over the past decade,[18–27] and can offer several advantages over steady-state techniques. These include decoupling of density and temperature gradients from each other, and a decoupling of temperature and density from their gradients, with no essential degradation of the quality of the data.[28]

It is important to point out the implicit difference between χ_e determined by perturbative techniques vs χ_e derived from steady-state power-balance methods. Perturbative techniques measure the change in heat flux induced by variations of the temperature gradient, producing $\chi_e\sim dq/d\nabla T_e$, where q denotes heat flux. Steady-state power-balance techniques, on the other hand, compare total fluxes and gradients, producing $\chi_e\sim q/\nabla T_e$. If χ_e exhibits a nonlinear dependence on temperature gradient (in particular if q is an increasing function of ∇T_e), a perturbative measurement will produce a higher χ_e value than a steady-state measurement. An excellent review of this subject is covered in Ref. 28.

Historically, χ_e values derived from perturbative techniques have exceeded χ_e derived from power balance by a

[a]Electronic mail: tmunsat@pppl.gov

factor of 1–5 or more. Nonlinear gradient dependence or fast nonlocal transport are typically cited as explanations for this discrepancy, though recent work has demonstrated that transient MHD activity may dominate these effects by introducing weak stochasticity to the local field structure.[29]

One feature of perturbative analysis that is particularly relevant to the CDX-U experiment is that of diagnostic instrumentation. For power-balance analysis, one is required to know with great certainty the profiles of electron temperature, ion temperature, electron and ion density, and all power sources and sinks, including ohmic heating and radiative losses. Though it is not necessary to know the time dependence of these quantities, *all* quantities must be known in order to calculate *either* of χ_e or χ_i. Transient techniques, by contrast, are critically dependent on time resolved data, but are only weakly dependent on absolute calibration and require only a subset of the above measurements to measure either χ_e or χ_i. Furthermore, the time-dependent analysis of plasma perturbations is performed when heat and particle sources and sinks can be ignored, which is the case if the sources and sinks are not time dependent with the perturbation. This type of analysis is well suited to CDX-U, which lacks T_i diagnostics and has only an uncalibrated estimate of radiated power, but is equipped with spatially and temporally resolved T_e diagnostics. The electron Bernstein wave (EBW) T_e diagnostic, while not absolutely calibrated, provides time-resolved profiles of radiation temperature, and the soft x-ray (SXR) array provides time-resolved $C(V)$ emission profiles.

II. HEAT-PULSE EXPERIMENTS USING SAWTEETH PERTURBATIONS

Electron thermal transport in CDX-U was assessed by recording the spatial and temporal evolution of sawtooth-induced perturbations with the SXR array.[30] SXR emission in CDX-U is almost exclusively due to line radiation, primarily from oxygen and carbon impurity ions. For this experiment a 0.3 μm Ti foil filter was used, which blocks out nearly all oxygen emission while admitting the brightest CV and CVI lines, which are exponentially dependent on T_e. Although the SXR data is not inverted for this study, the fact that the SXR intensity increases with all three parameters T_e, n_e, and n_C, all of which are peaked in CDX-U, means that each measurement will be heavily weighted by the innermost flux-surface intersected by the viewing chord. A layout of the array, including the intersection of the viewing chords with the CDX-U flux surfaces, is shown in Fig. 1. The r value for each viewing chord was calculated by taking the outermost flux surface intersected by the chord and mapping it back to the midplane, assuming that thermal transport along a magnetic surface is much faster than transport across compressed magnetic surfaces. The array is vertically symmetric about the midplane, so that the 30 viewing chords correspond to 15 radial observation locations: r_{obs} (cm)= 13.9, 13.0, 12.1, 11.2, 10.3, 9.4, 8.4, 7.5, 6.5, 5.5, 4.5, 3.5, 2.4, 1.4, 0.3.

The spatio-temporal evolution of a diffusion-dominated temperature perturbation is governed by the perturbed electron heat equation

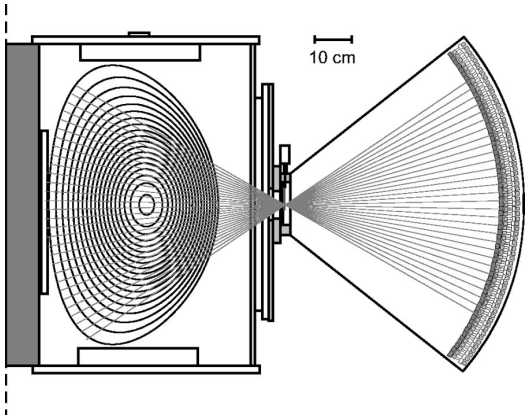

FIG. 1. Layout of SXR array, including viewing chords and CDX-U flux surfaces.

$$\frac{3}{2} n_e \frac{\partial \tilde{T}_e(r,t)}{\partial t} = \frac{1}{r} \frac{\partial}{\partial r}\left[r\, n_e\, \chi_e \frac{\partial \tilde{T}_e(r,t)}{\partial r}\right]. \tag{1}$$

In the case of sawteeth-induced perturbations, the initial conditions for this equation can be taken as a pair of opposing δ functions located at the inversion radius. An analytical solution to this equation with δ function initial conditions, as given in Ref. 31, is

$$\tilde{T}_e(r,t) = \frac{A^2 r_1 r_s \tilde{T}_{e0}}{2t} \exp\left(\frac{-A^2 r^2}{4t}\right) \times \left[\exp\left(\frac{-A^2 r_2^2}{4t}\right) I_0\left(\frac{A^2 r r_2}{2t}\right) - \exp\left(\frac{-A^2 r_1^2}{4t}\right) I_0\left(\frac{A^2 r r_1}{2t}\right)\right], \tag{2}$$

where t is the time measured from the sawtooth time t_s, r_s is the sawtooth inversion radius, r_0 ($\leqslant \sqrt{2} r_s$) is the reconnection radius, and r_1, r_2 are the positions of the negative and positive delta functions, respectively (each of magnitude $\tilde{T}_{e0}$), $A = \sqrt{1.5/\chi_e}$, and I_0 is a modified Bessel function of order zero.

An approximate solution to this equation, derived in Ref. 18, leads to a description of the perturbation trajectory given by

$$\Delta t_{\mathrm{peak}} \approx \frac{(\Delta r_{\mathrm{peak}})^2}{13.5 A^2} = \frac{(\Delta r_{\mathrm{peak}})^2}{9 \chi_e}, \tag{3}$$

where Δt_{peak} is the delay between the initial perturbation and the local measurement, and Δr_{peak} is the difference between the location of the local peak and the location of the initial perturbation.

In the CDX-U experiments, the raw SXR data was best-fit to the evolved perturbation function given by Eq. (2), parametrized by χ_e, t_s, r_{obs}, and a scalar magnitude. t_s and r_{obs} were fixed according to the location of the observed sawtooth, and χ_e was derived by finding a best-fit to the data at each measurement chord. A series of SXR wave forms

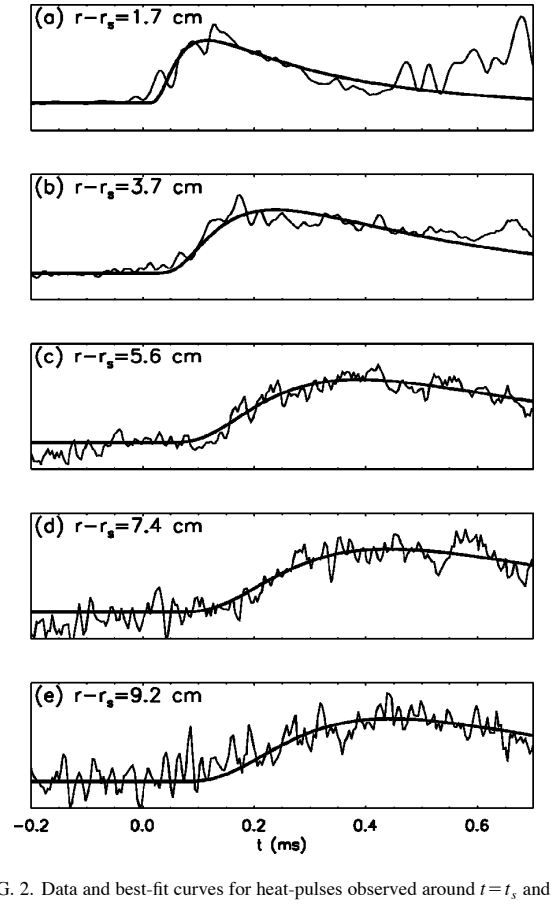

FIG. 2. Data and best-fit curves for heat-pulses observed around $t=t_s$ and at $r>r_s$, shot 0721001256. The radial difference between plots (a) and (d) is nearly identical to that between plots (d) and (e), though the pulse shape evolves significantly in the former case, and is nearly identical in the latter.

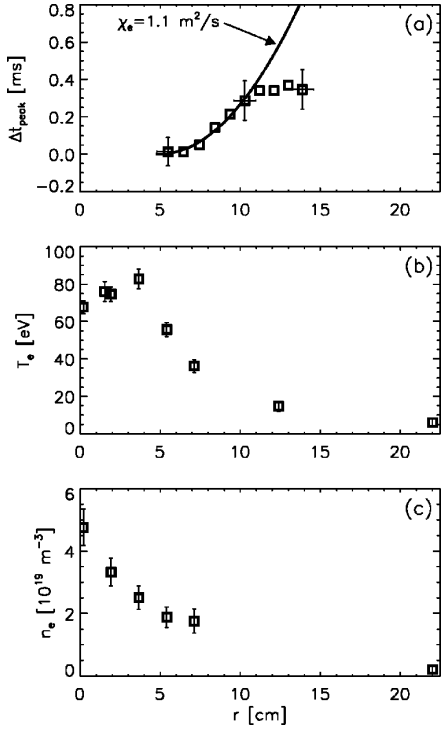

FIG. 3. Plot of heat pulse delay (a), electron T_e (b), and n_e (c) profiles versus minor radius. The heat-pulse trajectory is fit to a quadratic representing $\chi_e=1.1$ m^2/s for $r_s<r<10.5$ cm. The steep T_e gradient at $r/a\sim 1/3$ matches the region of inferred low χ_e. The n_e profile is peaked within the $q=1$ radius, as shown.

covering the full range of the SXR array outside the sawtooth radius, plotted with the best-fit solutions of Eq. (2) is shown in Fig. 2.

Similar perturbative studies on other devices have employed Fourier techniques and coherent averaging over series of sawteeth to reduce noise and to extract phase information from the traveling pulse. CDX-U discharges contain only a few sawteeth each, however, with a "flat-top" duration of $\lesssim$5 ms, and are therefore too short to enable such methods. Coherent pulse averaging was possible, though, by using series of similar discharges, resulting in substantial reduction of the noise in the averaged wave forms and an improved fit to the model curves. The wave forms in Fig. 2 were produced by averaging data from six similar discharges, synchronized to the sawtooth crash time t_s. Additionally, SXR chords from symmetric locations above and below the midplane have been averaged.

It is important to notice the progression from one channel to the next as the pulse travels from the $q=1$ surface outward. Channels at $(r-r_s)<5$cm demonstrate a pulse evolution well represented by Eq. (2) with $\chi_e=1.1$ m^2/s. While the Δr covered between Figs. 2(a) and 2(c) (3.9 cm) is nearly identical to that covered between Figs. 2(c) and 2(e) (3.6 cm), the pulse shape undergoes significant relaxation/delay over the first 3.9 cm, and almost no further evolution over the last 3.6 cm, indicating relatively rapid thermal transport through this outer region.

In order to illustrate this behavior more precisely, the Δt_{peak} values for each channel are plotted against the observation radius for that channel, producing a map of the pulse trajectory in space and time, shown in Fig. 3(a). Vertical error bars in Fig. 3(a) represent the uncertainty in the pulse peak time, given by $\sigma_t^2=(\int t^2 y\,dt)/(\int y\,dt)$, applied to the decay of the wave forms shown in Fig. 2.

The quadratic fit representing $\chi_e=1.1$ m^2/s [from Eq. (3)] accurately represents the heat pulse delay data only for $r_s<r<10.5$ cm, while χ_e is seen to increase sharply outside of this region.

Although it is difficult to assess a χ_e value in the outer region with reasonable precision, it appears to exceed the core value by an order of magnitude or more. Individual analysis of several similar sawtoothing discharges showed very uniform profile behavior, with derived χ_e values in the core ranging from 0.8 to 2.2 m^2/s.

Figures 3(b) and 3(c) show T_e and n_e profiles from the multichannel Thomson scattering (TVTS) diagnostic, supplemented by an edge measurement ($r=22$ cm) from a triple Langmuir probe. The steepest temperature gradient exists in the region of measured low χ_e ($r/a\sim 1/3$), and a much flatter

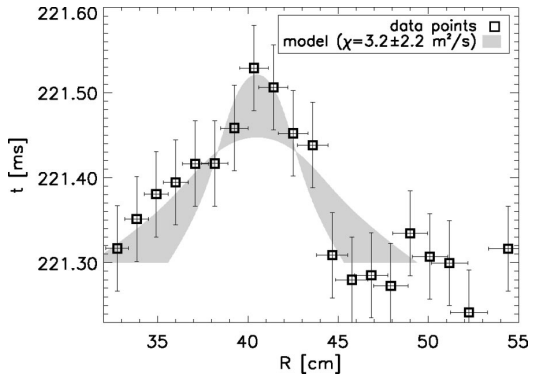

FIG. 4. Plot of heat pulse delay versus major radius, comparing χ_e model to data from fast-scanning EBW radiometer. The shaded region corresponds to model parameters covering $\chi_e = 3.2 \pm 2.2$ m^2/s and $r_{\text{perturbation}} = 7.6 \pm 3.3$ cm, i.e., a perturbation localized around $r_{\text{perturbation}}/a \sim 1/3$.

(and colder) region exists where χ_e is measured to be sharply higher.

The n_e profile [Fig. 3(c)] also exhibits a steep central gradient and peak, though the n_e gradient appears at smaller radius than the temperature gradient. The n_e peak, as well as the corresponding dip in T_e, appear within the $q=1$ radius, as indicated in the figure.

III. COLD-PULSE EXPERIMENTS USING EDGE GAS PUFFING

A complementary χ_e measurement was performed using similar time-to-peak methods applied to cold-pulses propagating inward from the plasma edge. For these experiments, gas-puffing modulations were introduced to a background plasma which acted to locally cool the edge, and the temperature response was measured using the electron Bernstein wave (EBW) T_e diagnostic.[32] The T_e perturbation was measured at the plasma edge with a triple Langmuir probe. A series of reproducible discharges was taken with the EBW radiometer scanning in frequency either shot-to-shot or many times within a single shot. The EBW frequency range was 8.4–12.4 GHz, corresponding to second-harmonic EBW emission covering $R = 35.7 - 53.3$ cm, roughly the center to the outer edge of the plasma. The triple probe was held fixed at the plasma edge ($R = 56$ cm) for all shots.

For experiments using the fast-scanning radiometer, the frequency was swept at 50 frequency sweeps per millisecond. Data was sampled at 1 MHz, providing 20 points per sweep, though the phase of the frequency sweep was uncorrelated with the phase of the sampling. EBW emission intensity vs time and frequency was interpolated over an irregular grid, and data from several identical shots were summed to improve signal-to-noise levels. The combined data was then regridded to provide a set of time traces at fixed frequency locations (each corresponding to a radius in the plasma). The local minimum at the cold pulse was then located for each radius. The resulting dataset is shown in Fig. 4.

Because of the regridding process, interpolated time traces were produced at several hundred radius locations. In order to faithfully represent the original sampling rate (and not present falsely high resolution in the data points), the analyzed data was rebinned into 20 evenly spaced radial locations.

To model the edge perturbations, Eq. (1) was numerically solved using a time-dependent boundary condition at the plasma edge corresponding to a negative temperature perturbation. The subsequent relaxation over the plasma profile was evolved in time, and from this the trajectory of the perturbation peak was plotted to provide a straightforward means of comparison to experiment. Plotted with the data is the result of the simulation over the ranges $\chi_e = 1.0 - 5.4$ m^2/s and $r_{\text{perturbation}} = 5.3 - 9.9$ cm.

Error bars in major radius (R) were produced by perturbing each of the quantities used to provide the mapping between frequency and major radius, namely B_T and $I_P(r)$, by their estimated error, and also taking into account the error introduced by the finite bandwidth of the radiometer electronics. Each contribution to the overall error in R was then added in quadrature, though in practice the radiometer bandwidth dominated the other effects. Errors in time represent the scatter in the derived temperature peaks within each bin of overgridded time traces.

The reasonable fit between the data and model implies that thermal transport in the CDX-U core can be described by a diffusive process, with a diffusion coefficient of $\chi_e \sim 3$ m^2/s. An additional important result comes from the fact that the data is well modeled by a perturbation originating around $r = 7.5$ cm, corresponding to $r/a \sim 1/3$. Outside this region, the data points are quite flat, which implies either that the diffusive transport is very fast beyond $r = 7.5$ cm, or that the perturbation introduced by the cold-pulse is not diffusive outside the plasma core. This observation is similar to the sawtooth-induced heatpulse propagation results in Sec. II.

Similar cold pulse experiments were performed using a slightly different experimental arrangement, with similar results. In these sets, the EBW radiometer sampled a single frequency during each shot, and was scanned between shots over the range 8.4–12.4 GHz over the course of several similar shots. This provided a higher sampling rate at each frequency, but lacked single-shot profile information. In these sets, a record of the pulse at the plasma edge was recorded by either the triple Langmuir probe or by a second EBW radiometer at a fixed reference frequency corresponding to the plasma edge. Analysis of these data sets resulted in $\chi_e = 1.5 - 5.9$ m^2/s and $r_{\text{perturbation}} = 5.5 - 9.5$ cm, corresponding to $r_{\text{perturbation}}/a = 0.25 - 0.43$. As in the previous set, the data fits the model reasonably well inside the core and flattens out beyond $r/a \sim 1/3$, indicating an increase in transport outside the core.

In experiments such as these in which the temperature is perturbed through fueling modification, it is critical to investigate the possibility of coupling between the density and temperature perturbations, and the effect that it will have on the measured diffusion coefficients. A mathematical outline of the coupling between density and temperature perturbations and the effect of off-diagonal elements in the transport matrix is given in Ref. 33. The primary finding of this work is an analytical treatment of the effect that gradient-dependent transport coefficients will have on perturbative

measurements as compared to steady-state methods. It is also found that coupling of the temperature and density perturbations can lead to a separate "fast" and "slow" eigenmode solution to the diffusion equation, with corresponding pulse propagation rates.

In the CDX-U experiments, separate propagation eigenmodes were not observed, though the quality of the data may not be sufficient to resolve subdominant pulses or to resolve the possible coupling between n_e and T_e pulses. In particular, the edge cold-pulse experiment is the most susceptible to coupling between n_e and T_e diffusion, since the T_e perturbation is a direct consequence of an induced n_e perturbation. Indeed, the χ_e values from the edge cold pulses were consistently higher than those determined from the sawtooth analysis, consistent with a finite coupling effect. Although localized n_e wave forms are not available, microwave-interferometer data representing $\int n_e$ (line integrated through the plasma center) indicate $\sim 4\%$ total modulation during the gas-pulse injection.

Additionally, an alternative explanation for the enhanced transport outside of the core is that of neutral penetration from the source gas puff. Franck–Condon neutrals penetrating from the edge with energy of ~ 2 eV will penetrate the outer 2/3 of the plasma in ~ 15 μs, consistent with the experimental observation of the pulse propagation through this region. However, when the cold pulse results are considered in combination with the similar results from the sawtooth study, in which the perturbation was induced by a different mechanism with propagation in the opposite direction, neutral-penetration effects cannot account for the apparent χ_e profile.

IV. DISCUSSION

In trying to determine the source of the sharp transition in transport behavior observed in CDX-U, it is important to consider the possibility that transport is locally enhanced by a large magnetic island. In CDX-U, evidence for magnetic islands is obtained with both the SXR array and the scanning microwave interferometer, both of which sample nearly the full plasma radius. Additional information may be provided by the triple probe, located at $r=22$ cm, and the Mirnov coils at the vessel wall.

Representative spectra of the SXR signal fluctuations, taken at $r=4.5$ cm and 10.3 cm (chosen to best represent the low and high χ_e regions while remaining above the noise floor), are shown in Fig. 5. The spectra have been normalized to the mean signal level for each channel. Also shown is the noise-floor imposed by amplifier noise and digitization bit-noise, calculated by using signals from the SXR array recorded before the plasma shot. [A photon-noise floor was also calculated, but is negligible compared to both the signal level in Fig. 5(a) or the bit-noise floor in Fig. 5(b).]

Fluctuations at $r=4.5$ cm show the $q=1$ island at ~ 10–12 kHz and harmonics. The $q=1$ island is typical of CDX-U plasmas, and is pervasive even in non-sawtoothing discharges. Fluctuations at $r=10.3$ cm exhibit nearly white noise, reaching a noise floor at $\sim 10^{-4}$. Importantly, the frequency band $f<20$ kHz is above the noise floor in both

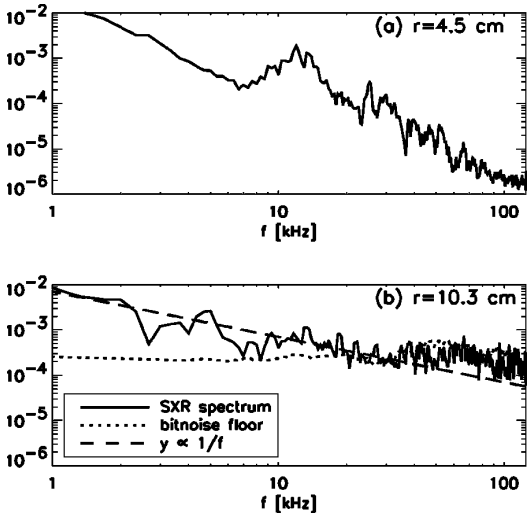

FIG. 5. Fluctuation spectra of the SXR signals, taken at two representative radii; (a) $r=4.5$ cm and (b) 10.3 cm represent the low and high χ_e regions, respectively. Fluctuations at $r=4.5$ cm show the $q=1$ island at ~ 10 kHz and harmonics. Fluctuations at $r=10.3$ cm exhibit nearly "white" noise, lower than the preceding plot by two orders of magnitude or more, reaching a noise floor at $\sim 10^{-4}$. Fluctuation levels at $r=10.3$ cm, measurable above the noise floor for $f<20$ kHz, are similar to or lower than the corresponding levels at $r=4.5$ cm.

plots, and the relative fluctuation level in the high χ_e region is equal to or lower than that in the low χ_e region.

Similar analysis was performed on signals from a microwave interferometer, scanned (shot-to-shot) from the plasma center to the edge, as well as on signals from a triple Langmuir probe at the plasma edge (both sampled at 100 kHz). Neither diagnostic showed evidence for magnetic islands outside of the $q=1$ surface, and the interferometer scan showed comparable fluctuation levels in the high and low confinement regions. Additionally, spectral analysis of the Mirnov-coil array at the vessel wall showed dominant 10 kHz activity, corresponding to the $q=1$ island.

The dominant MHD activity in CDX-U appears to be the $q=1$ magnetic island, located well within the higher confinement region. Given the magnitude of this island and the size of the high χ_e region, it would seem that any magnetic island capable of causing the observed transport transition would need to be quite significant, though the fluctuation analysis shows no evidence of a magnetic island in the vicinity of the χ_e transition.

Although it is widely believed that microturbulence of one form or another is the dominant mechanism leading to measured transport coefficients, it is nonetheless useful to maintain a comparison of any experimental data with neoclassical estimates. In particular, it has been predicted that the ST geometry may lead to stabilization of low-n MHD modes.[2,8] Though tokamak experiments have yet to achieve neoclassical electron confinement, both neoclassical ion thermal confinement[7,34] and ion particle confinement[35] have been observed. Additionally, core electron thermal transport barriers have been observed in both DIII-D and RTP with auxiliary electron heating, though even in these cases electron

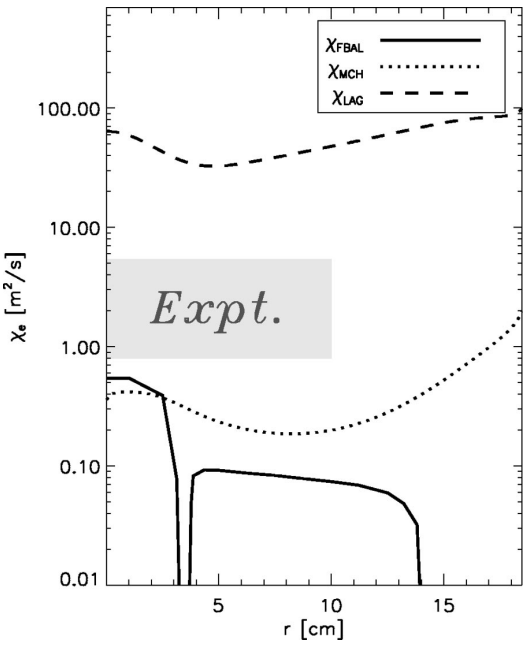

FIG. 6. χ_e models and experimental data. χ_{FBAL} is the neoclassical estimate from the FORCEBAL code, χ_{MCH} is the modified Chang–Hinton estimate, and χ_{LAG} is the Lackner–Gottardi model. The shaded region encompasses the range of χ_e measurements from the temperature pulse experiments. The measurements also demonstrate sharply higher χ_e for $r>10$ cm.

thermal transport remained anomalously high.[36,37]

Neoclassical estimates of all transport coefficients have been well established for high aspect ratio geometry, often using inverse aspect ratio as an expansion parameter in the derivation by Hirshman.[38] The commonly used Chang–Hinton expression for χ_i which incorporates finite aspect-ratio effects and interpolates between different collisionality regimes is given by Chang *et al.*[39] Neoclassical estimates for χ_e which include finite aspect-ratio effects and span all collisionality regimes have recently been developed by Houlberg,[40] and incorporated into the NCLASS and FORCEBAL codes.

The solid line in Fig. 6, labeled χ_{FBAL}, shows the χ_e estimates calculated by the FORCEBAL code, using the profiles shown in Fig. 3 and a magnetic equilibrium geometry produced by the EFIT code for these shots. The shaded region in Fig. 6 represents the full range of measured χ_e values from the temperature pulse measurements. Though not shown in the figure, recall that the experiments also demonstrate a sharp increase in χ_e for $r>10$ cm.

Clearly χ_{FBAL} is a very poor match to the measured χ_e, both in magnitude and profile shape. The measured χ_e is 10 times higher than χ_{FBAL} in the core, and the qualitative experimental evidence for increased edge transport bears no resemblance to the χ_{FBAL} profile.

Interestingly, if the Chang–Hinton expression for χ_i is modified for electrons, by replacing all ion quantities (ν_i, ρ_i, etc.) with the corresponding electron quantities, the resulting χ_e profile shape matches the CDX-U data somewhat more closely. The result of this calculation is shown in Fig. 6, labeled χ_{MCH}, along with a second scaling, labeled χ_{LAG} and described below. The modified Chang–Hinton expression χ_{MCH} is 5 times lower than the measured CDX-U value, somewhat comparable to the result obtained using FORCEBAL. The profile is a closer match to the CDX-U data, though the χ_{MCH} estimate places the χ_e gradient at a slightly larger r value than that measured in CDX-U.

Also shown in Fig. 6 is the semiempirical Lackner–Gottardi χ_e model, labeled χ_{LAG}. This curve uses the form modified by Connor for low aspect-ratio,[15,16] which has been used in past comparisons to START transport data. The χ_{LAG} scaling is intended for ohmic and L-mode plasmas, based on a simple model in which trapped particles are displaced by a banana width on each bounce.

χ_{LAG} reproduces the measured χ_e profile very poorly, and also overestimates the minimum χ_e by a factor of 40. Interestingly, this is the model that has produced the best agreement with START power-balance based χ_e data, in magnitude if not always in profile shape. It should also be noted that in the START high-performance NBI-heated discharges, the χ_{LAG} estimates were very close to those calculated for CDX-U, though in that case the χ_{LAG} estimates were a much closer match to the experimental χ_e values.[7]

In general, the comparisons to the two neoclassical and one semiempirical χ_e estimates is quite unsatisfactory. Only one model (modified Chang–Hinton expression) seems to vaguely represent the measured χ_e behavior, and even this is a factor of 5 too low. Interestingly, the models chosen both underestimate and overestimate the measured χ_e. With the estimates covering such a wide range of predictions, it is difficult to draw concrete conclusions from the comparisons.

Although the lack of T_i and P_{rad} profile data prevents a local power-balance calculation, one can generate an approximate global χ_e^{GLO} estimate, useful for comparisons with other experiments.[20] Using the expression $\chi_e^{\mathrm{GLO}}=(\kappa a^2)/(4\tau_E)$, where $\tau_E=E_{\mathrm{stored}}/(P_{\mathrm{OH}}-P_{\mathrm{rad}})$, E_{stored} is the total stored kinetic energy and $(P_{\mathrm{OH}}-P_{\mathrm{rad}})$ is the total input power, one finds $\chi_e^{\mathrm{GLO}}=33$ m^2/s, far higher than the result from the perturbative analysis. The T_e, n_e, and perturbative χ_e profiles all indicate that the vast majority of confined energy is within $r/a\sim 1/3$, though, and indeed if a is replaced with $a/3$ in the expression for χ_e^{GLO}, and only the stored energy within $r=a/3$ is considered ($\sim$70% of the total), the result is $\chi_e{}^{\mathrm{GLO}}=2.4$ m^2/s, consistent with the perturbative experiments. For this calculation, the quantities $T_i=0.7\,T_e$ and $P_{\mathrm{rad}}=0.3P_{\mathrm{OH}}$ were assumed, but the results do not qualitatively change over the ranges $0.5\leqslant T_i/T_e\leqslant 0.9$ and $0.1\leqslant P_{\mathrm{rad}}/P_{\mathrm{OH}}\leqslant 0.5$. Calculated over these parameter ranges, $\chi_e^{\mathrm{GLO}}=21-48$ m^2/s using the full plasma volume, and $\chi_e{}^{\mathrm{GLO}}=1.9-3.4$ m^2/s using only the volume within $r=a/3$, again consistent with the perturbative results.

As mentioned above, the sole χ_e profile estimate in an ST was performed on START,[7] with a result that is substantially higher ($\sim$20–30 m^2/s) than the CDX-U value in the core. Interestingly, the χ_e^{GLO} calculated above for the full CDX-U plasma volume is comparable to the START estimates, though this has limited significance due to the large differences in the χ_e profiles between the two machines.

Although the geometry of CDX-U and START are somewhat similar, one important difference is the heating method: ohmic heating in CDX-U, and neutral-beam injection (NBI) in START. In CDX-U, the electron-ion thermal equilibration time is the same order as the energy confinement time, and it has therefore been estimated that T_i is significantly lower than T_e. In START, by contrast, measurements in NBI plasmas have shown $T_i \approx T_e$.

Recent linear gyrokinetic simulations have shown that destabilization of electron temperature gradient (ETG) modes can depend critically on the ratio $\tau \equiv T_e/T_i$.[41] For a given configuration, higher τ leads to a stabilization of ETG modes and a destabilization of ion temperature gradient (ITG) modes, which would result in enhanced energy loss through the ion channel. Conversely, lower τ leads to stabilization of ITG modes and a destabilization of ETG modes, resulting in energy loss through the electron channel. This trend would correspond to predominant ion thermal loss in the CDX-U case and predominant electron thermal loss in the START case. In order to make quantitative estimates of the critical T_e gradients which would lead to ETG destabilization, it is necessary to know the T_i profile, which is unfortunately unavailable on CDX-U. On the other hand, this mechanism does present a possible scenario that is consistent with the contrasting results from CDX-U and START.

An alternative explanation for the observed CDX-U χ_e behavior is the existence of a thermal transport barrier near $r=a/3$. Though this conjecture is impossible to verify without velocity profile information, it should be noted that ST's are predicted to have relatively high rotation velocity, which could lead to layers of turbulent eddy suppression and formation of a thermal transport barrier.

In summary, the electron transport profile has been measured in CDX-U using two independent perturbative methods, representing the first local measurements of χ_e in a spherical torus. Core ($r/a<1/3$) χ_e values from the sawtooth study are 1–2 m^2/s, and from the gas modulation study are 1–6 m^2/s, increasing by an order of magnitude or more outside of the core region. T_e profiles exhibit steep gradients in the region of low measured χ_e, reaffirming the conclusion of distinct regions of high and low transport levels. It appears from all available diagnostics that the profile behavior is not caused by a degradation of confinement due to the presence of a magnetic island. Though D_e was not measured explicitly in these experiments, the n_e profiles also exhibit steep gradients in the core region, at a measurably different radius than the thermal gradients. Specifically, the n_e peak appears inside the $q=1$ radius, and the T_e gradient region appears outside of $q=1$. The location of other rational q surfaces has not been measured in these plasmas.

The measured χ_e level is a factor of 5–10 higher than neoclassical estimates, with a poor match to the profile shape. Likewise, a semiempirical χ_e scaling which has shown somewhat favorable comparison to START electron transport data shows poor agreement with the CDX-U experimental results.

Several studies have been performed on other tokamaks which indicate that χ_e measured by perturbative techniques can be several times higher than that determined by power-balance techniques, due to nonlinearities in the dependence of χ on ∇T, local MHD perturbations, or coupled n_e and T_e diffusion. Comparison with neoclassical χ_e calculations indicate that the experimental values in CDX-U are 5–10 times higher than neoclassical estimates, though the steady-state experimental value may be closer than this.

ACKNOWLEDGMENTS

The authors would like to acknowledge E. Fredrickson, D. Hoffman, B. LeBlanc, and J. Taylor for their contributions to this research.

This work was supported by U.S. Department of Energy Contracts Nos. DE-AC02-76CH03073 and DE-FG02-99ER54523.

[1] Y.-K. Peng and D. Strickler, Nucl. Fusion **26**, 769 (1986).
[2] R. Stambaugh, V. Chan, R. Miller, and M. Schaffer, Fusion Technol. **33**, 1 (1998).
[3] J. Menard, S. Jardin, S. Kaye, C. Kessel, and J. Manickam, Nucl. Fusion **37**, 595 (1997).
[4] R. Miller, Y. Lin-Liu, A. Turnbull, V. Chan, L. Perlstein, O. Sauter, and L. Villard, Phys. Plasmas **4**, 1062 (1997).
[5] T. Hender, L. Baker, R. Hancox, J. Hicks, P. Knight, D. Robinson, and H. Wilson, in *Proceedings of the 14th International Conference on Plasma Physics and Controlled Nuclear Fusion Research, Wurzburg, 1992* (IAEA, Vienna, 1992), Vol. 3, p. 339.
[6] M. Gryaznevich, R. Akers, P. Carolan *et al.*, Phys. Rev. Lett. **80**, 3972 (1998).
[7] D. Gates, R. Akers, L. Appel *et al.*, Phys. Plasmas **5**, 1775 (1998).
[8] G. Rewoldt, W. Tang, S. Kaye, and J. Menard, Phys. Plasmas **3**, 1667 (1996).
[9] A. Sykes, R. Akers, L. Appel *et al.*, Phys. Rev. Lett. **84**, 495 (2000).
[10] Y.-K. Peng, Phys. Plasmas **7**, 1681 (2000).
[11] M. Ono, S. Kaye, Y. Peng *et al.*, Nucl. Fusion **40**, 557 (2000).
[12] A. Sykes, J. Ahn, R. Akers *et al.*, Phys. Plasmas **8**, 2101 (2001).
[13] R. Colchin, P. Carolan, R. Duck *et al.*, Phys. Fluids B **5**, 2481 (1993).
[14] M. Walsh, R. Bamford, P. Carolan *et al.*, in *Proceedings of the 22nd European Physical Society Conference on Controlled Fusion and Plasma Physics, Bournemouth, England 1995* (European Physical Society, Geneva, 1995), Vol. 3, p. 33.
[15] C. Roach, Plasma Phys. Controlled Fusion **38**, 2187 (1996).
[16] K. Lackner and N. Gottardi, Nucl. Fusion **30**, 767 (1990).
[17] T. Jones, Ph.D. thesis, Princeton University, 1995.
[18] E. Fredrickson, J. Callen, K. McGuire *et al.*, Nucl. Fusion **26**, 849 (1986).
[19] E. Fredrickson, K. McGuire, A. Cavallo *et al.*, Phys. Rev. Lett. **65**, 2869 (1990).
[20] B. Tubbing, N. L. Cardozo, and M. V. D. Wiel, Nucl. Fusion **27**, 1843 (1987).
[21] M. Kissick, E. Fredrickson, J. Callen *et al.*, Nucl. Fusion **34**, 349 (1994).
[22] K. Gentle, G. Cima, H. Gasquet *et al.*, Phys. Scr. **52**, 411 (1995).
[23] H. Walter, U. Stroth, J. Bleuel *et al.*, Plasma Phys. Controlled Fusion **40**, 1661 (1998).
[24] L. Giannone, V. Erckmann, U. Gasparino *et al.*, Nucl. Fusion **32**, 1985 (1992).
[25] U. Gasparino, V. Erckmann, H. Hartfuß, H. Maaßberg, and M. Rome, Plasma Phys. Controlled Fusion **40**, 233 (1998).
[26] P. Efthimion, C. Barnes, M. Bell *et al.*, Phys. Fluids B **3**, 2315 (1991).
[27] E. Synakowski, P. Efthimion, G. Rewoldt *et al.*, Phys. Fluids B **5**, 2215 (1993).
[28] N. L. Cardozo, Plasma Phys. Controlled Fusion **37**, 799 (1995).
[29] E. Fredrickson, M. Austin, and R. Groebner, Phys. Plasmas **7**, 5051 (2000).
[30] D. Stutman, J. Menard, Y.-S. Hwang, W. Choe, and M. Ono, Rev. Sci. Instrum. **68**, 1059 (1997), part II.
[31] M. Soler and J. Callen, Nucl. Fusion **19**, 703 (1979).

[32]G. Taylor, P. Efthimion, B. Jones *et al.*, Rev. Sci. Instrum. **72**, 285 (2001).
[33]K. Gentle, Phys. Fluids **31**, 1105 (1988).
[34]F. Levinton, M. Zarnstorff, S. Batha *et al.*, Phys. Rev. Lett. **75**, 4417 (1995).
[35]P. Efthimion, S. V. Goeler, W. Houlberg *et al.*, Nucl. Fusion **39**, 1905 (1999).
[36]C. Greenfield, C. Rettig, G. Staebler *et al.*, Nucl. Fusion **39**, 1723 (1999).
[37]M. deBaar, M. Beurskens, G. Hogeweij, and N. Cardozo, Phys. Plasmas **6**, 4645 (1999).
[38]S. Hirshman and D. Sigmar, Nucl. Fusion **21**, 1079 (1981).
[39]C. Chang and F. Hinton, Phys. Fluids **29**, 3314 (1986).
[40]W. Houlberg, K. Shaing, S. Hirshman, and M. Zarnstorff, Phys. Plasmas **4**, 3230 (1997).
[41]F. Jenko, W. Dorland, and G. Hammett, Phys. Plasmas **8**, 4096 (2001).